Acta Astronautica 208 (2023) 355–366

Contents lists available at ScienceDirect

Acta Astronautica

journal homepage: www.elsevier.com/locate/actaastro

Orbital kinematics of conjuncting objects in Low-Earth Orbit and opportunities for autonomous observations

Giulio Campiti [a], Giuseppe Brunetti [a], Vitali Braun [b], Eugenio Di Sciascio [a], Caterina Ciminelli [a,*]

[a] Department of Electrical and Information Engineering, Polytechnic University of Bari, Via E. Orabona 4, 70125, Bari, Italy
[b] IMS Space Consultancy at ESA/ESOC Space Debris Office, Robert-Bosch-Straße 5, 64293, Darmstadt, Germany

ARTICLE INFO

Keywords:
Autonomous collision avoidance
Space traffic management
Space situational awareness
Conjunctions
Onboard sensor

ABSTRACT

As satellites and debris continue to proliferate in Low Earth Orbit (LEO), collision avoidance maneuvers are becoming routine for operational spacecraft, causing increasingly discontinuous operations. Despite the congested environment, collisions are still very unlikely events and most satellites would never actually need to maneuver during their lifetime. Maneuvers are currently performed far more than necessary because of the limited accuracy of the tracking data used for assessing collision risks, which leads to overestimates. A little explored solution is to equip satellites with sensors that enable them, whenever at risk of collision, to autonomously track the hazardous objects and refine their positional knowledge before making a maneuver decision. Unlike what is possible from ground, satellites can collect data and estimate the collision risk even shortly before a potential collision (e.g., one orbit before), improving the final prediction accuracy and reducing false alarm rates. Moreover, while most surveillance data is currently obtained through ground-based sensors, space-based observations can provide unique information as they do not suffer from atmospheric issues (e.g., diffractions, aberrations). Here, the feasibility of observing hazardous objects directly from at-risk satellites before potential collisions is corroborated by demonstrating that objects in LEO usually pass close together several times before the closest approach, providing short observation opportunities. A thorough characterization of these observing windows is performed by reconstructing and analyzing the trajectory evolution for thousands of historical conjunction events, starting from Two-Line Element (TLE) sets and using a Simplified General Perturbations 4 model (SGP4) for the propagation. Statistical analysis is performed to assess the average number and duration of the observation opportunities, the relative distances and velocities involved, and other relevant features. Results show that a satellite with a detection range of 500 km would be able in more than 80% of the cases to observe a high-risk object twice and for at least 10 s before the potential collision.

1. Introduction

As the launch rate keeps accelerating and objects accumulate around the Earth, in-orbit collisions become increasingly probable and difficult to manage. Currently, risky close approaches (or conjunctions) are identified using tracking data mainly generated by ground-based sensors, which are able to regularly track all Resident Space Objects (RSOs) approximately larger than 10 cm [1]. With the current levels of space population, operators at European Space Agency (ESA) already deal with hundreds of conjunctions per week for each spacecraft [2], which eventually leads to the execution of two collision avoidance maneuvers per spacecraft per year [3]. Whenever a maneuver is performed, some propellant is lost to move the satellite and the onboard science instruments are typically switched off, causing a temporary interruption of nominal operations [3]. On May 16, 2022, five scheduled data downlinks of ESA's Copernicus Sentinel 1–A satellite had to be canceled to avoid a potential collision [4]. As the annual number of launched payloads has quadrupled in just the last four years [5], maneuvers are inevitably becoming more frequent, causing more discontinuous satellite operations and increasing revenue losses for spacecraft owners/operators (O/Os).

However, the actual chances of a satellite being struck by debris large enough to cause appreciable damage are very low [6] and will remain so for at least the foreseeable future. ESA's MASTER-8 model [7] for the space debris environment predicts that the impact rate of objects larger than 1 cm on a cross-section of 30 m^2 orbiting at 800 km of altitude (i.e.,

* Corresponding author.
E-mail address: caterina.ciminelli@poliba.it (C. Ciminelli).

https://doi.org/10.1016/j.actaastro.2023.04.032
Received 31 January 2023; Received in revised form 7 April 2023; Accepted 16 April 2023
Available online 18 April 2023

the most crowded region) is once every 101 years on average [8]. The reason why satellites are in practice maneuvered much more frequently is because of the uncertainty present in the surveillance data used to calculate collision risks and take maneuver decisions. Low confidence data result in larger collision probabilities and thus higher maneuvering rates. As estimated in Ref. [9], if the position of tracked objects was known with a precision of 10 m in all directions, a Sentinel-2 satellite would need to maneuver about once every 40 years. Therefore, in view of the future levels of space traffic, improving the quality of orbital information is essential to reduce the rate of false alarms and unnecessary maneuvers.

Some experiments have shown that combining Space Situational Awareness (SSA) data from different providers, including public and private ones as well as space operators, can substantially enhance the knowledge of objects' position and thus the accuracy of conjunction predictions [10,11]. However, the establishment of a reliable and large-scale data-sharing framework is a complicated matter, since several behavioral and psychological barriers can intervene that prevent the collaborative sharing of authoritative data between diverse entities. Political rivalries between governments, cross-cultural differences and the competitive and economic advantages of possessing unique SSA information are some of the factors hindering the process [12]. Another possibility, raised by several authors in the last decade, is to use ground-based laser ranging stations to make high-precision measurements of uncooperative RSOs and refine their positional accuracy [9,13–15]. Although early studies have demonstrated the potential of this technique, different constraints reduce the possibilities of making valuable observations, such as weather conditions, targets illumination and stations availability [15,16]. In parallel, solutions involving space-based sensors have recently gained interest as they overcome some limitations of their ground-based counterparts, such as the dependence on circadian rhythms and the presence of atmosphere-related problems (e.g., attenuation, absorption, diffraction) [17]. Most related research focuses on generally improving the current SSA capability by exploiting the unique observation possibilities available from space, for example by using in-situ sensors for the detection of uncatalogued millimeter-sized particles [18–20].

A more focused strategy to improve data accuracy for conjunction events is to equip satellites with sensors that enable them, whenever on-ground systems predict that they are at risk of upcoming collision, to independently track the hazardous secondary objects during the orbits prior to the predicted events. Before initiating observations, an at-risk satellite would be first provided with the estimated orbit of its secondary object as obtained from the ground, serving as the initial solution to be refined onboard by processing the tracking data acquired from space. The uplinked initial solution would also allow the satellite to identify a limited region of space from where the secondary object can be expected to appear at each observation opportunity, thus allowing the onboard sensor to be oriented wisely. Unlike ground operations, where the final maneuver decision must be taken much earlier due to the limited available slots for command uplink [21], a satellite can keep collecting data and assess the collision risk until very shortly before the Time of Closest Approach (TCA). By reducing the time between orbit determination and TCA, the future state of the secondary object can be predicted with a greater confidence level, leading to a smaller computed collision probability and a more informed maneuver decision [2]. In a recent experiment by the Canadian Space Agency, the NEOSSat satellite was able to successfully track objects in close approach with itself during the orbits prior to the closest passages, giving some proof of feasibility for the above strategy [22]. As evidenced by the authors, observing opportunities arose from the fact that most objects made multiple, decreasing-range approaches with NEOSSat before TCA, typically at a regular frequency of twice per orbit. Although this peculiar behavior could potentially provide a viable basis for an autonomous avoidance system, it has not been further investigated since.

The purpose of this paper is to more comprehensively study the kinematics of conjuncting objects before the closest approach, in order to assess how generalizable NEOSSat's results are and lay the grounds for a space-based observation strategy. To this end, an analysis of the trajectory evolution for past conjunction events during the two days leading to TCA is performed. To obtain statistically significant results, orbital data are extracted for about 22,000 conjuncting objects in the form of Two-Line Element (TLE) sets [23]. Each trajectory is reconstructed using the Simplified General Perturbations 4 (SGP4) model [24], the analytical propagator designed for use with TLEs. The time evolution of the relative distance, relative velocity and angular rate is computed for each event, to assess how common repeated encounters are before TCA and under what conditions they can translate into observing opportunities for satellites equipped with a secondary payload. Several aspects of such encounters are characterized, such as their duration and the angular rates involved.

2. Operational concept and sensor considerations

Before delving into the kinematic aspects of space conjunctions, a more detailed description of the operational concept behind the proposed avoidance system is provided in this section, along with some key considerations on the sensing element. In the following, the term "primary" refers to a generic satellite hosting the system and "secondary" identifies an object involved in a conjunction with the primary.

The onboard system is intended to execute a series of sequential actions that are triggered whenever a new upcoming conjunction involving the primary is identified by the ground-based systems. The timing of first conjunction identification may differ depending on the particular service that the spacecraft O/O is relying on for obtaining orbital safety information. The U.S. Space Force's 18th Space Defense Squadron (SDS), which has historically provided free conjunction information to the space community, makes predictions up to 7 days in advance [25]. Following the first identification, the orbital data available for the secondary is initially transmitted to the primary satellite. Provided that the latter has self-position awareness (e.g., through a GNSS receiver), the onboard processing capabilities are utilized to propagate both objects' states forward in time and determine the first available time window for conducting on-site observations. One possible criterion to identify data collection opportunities is to calculate when the relative distance between the objects falls below a certain threshold (e.g., 300 km), selected according to the onboard sensor's detection capabilities. A second essential function of the uplinked orbital data is to enable the satellite to calculate the restricted region of space where the secondary can be expected to be visible upon approaching. Thus, at each planned observation, the satellite properly orients the sensor's Field of View (FoV) in the direction of the oncoming object and attempts to track it. Depending on the approach geometry, it may sometimes be more convenient in terms of attitude control demands to observe the object as it is receding rather than approaching. The acquired data are used onboard to refine the available knowledge on the secondary object using a sequential filter orbit determination process, which allows the orbital state to be updated in real-time with each new observation. It should be noted that, in parallel to this process, the secondary object will still be detected by the traditional ground-based SSA systems and its orbit will continue to be estimated by entities such as the 18th SDS. As long as it is possible, those orbital solutions should be provided to the primary during its scheduled ground-station accesses. One of the reasons is that observation attempts from space may prove unsuccessful for various causes, such as the object being in a different position than expected or being too dim to be detected by the onboard instrument. Should the primary fail to collect any data, an autonomous maneuver decision cannot be made by only relying on the orbital estimate uplinked at the time of first event identification. That data could be several days old, and the uncertainties about an object's position rapidly grow the farther in time its orbit is propagated. Additionally, combining the latest ground-derived solutions with the self-obtained observations is what

Action	NORAD Catalog Number	Name	Days Since Epoch	Max Probability	Dilution Threshold (km)	Min Range (km)	Relative Velocity (km/sec)
				Start (UTC)	TCA (UTC)	Stop (UTC)	
TLE Data	45437	ONEWEB-0092 [+]	1.145	1.708E-04	0.065	0.094	14.378
	31990	FENGYUN 1C DEB [-]	1.804	2023 Jan 12 06:55:32.784	2023 Jan 12 06:55:33.132	2023 Jan 12 06:55:33.479	

Fig. 1. Data reported by SOCRATES for a conjunction predicted for January 12, 2023 [25].

ensures that the onboard available solution is always more accurate, or at most the same, than that of ground, ultimately leading to an improvement over the current process.

At a certain point in time, the whole process of collecting data, refining the orbit solution and updating the collision risk is entirely moved to the space segment. The precise timing can be decided in different ways based on operators' needs and/or preferences. One option is to let the satellite autonomously handle the process only after the last ground-station access before TCA, or after one of the last ones. Another option is to set a fixed time before the TCA (for example, 1–2 days). In this regard, it is worth noting that many operators typically make a final maneuver decision more than 3 days before the event, as evidenced in a recent survey among the members of the Space Data Association [26]. Letting the satellite take care of improving the decision in the remaining 3 days would certainly decrease false alarm rates. In any case, the final maneuver decision is made by the primary in the very last orbits before TCA, waiting as long as possible to get a better estimate but still allowing enough time to implement an efficient maneuver.

A key component of the considered autonomous system is the onboard sensor, which should track distant objects (>100 km) traveling at velocities in the order of km/s. Unless a satellite is already equipped with a suitable sensor, a dedicated secondary payload should be embarked onboard. This may be reasonable only for satellites weighting at least a few hundred kilograms, where a small additional payload would represent a tiny fraction of the overall mass. Those satellites are also the most important to protect, given their high economic value and because they are more exposed to collision risks than the smaller satellites. The target objects of the observations are all those that can be detected from ground and are deemed risky for the satellite hosting the sensor. Their minimum size is therefore currently limited to about 10 cm, but will reduce to a few centimeters in the coming years thanks to the ongoing improvements in ground surveillance capabilities [1].

Both active and passive sensor technologies could be considered for the sensing element. Active sensors, such as radars or Light Detection and Ranging (LiDAR) systems, work by illuminating target objects and measuring the reflected energy coming back. These sensors have the major advantage of being independent of external light sources. Radars have been widely proposed as primary payloads for applications of debris monitoring, but their Size Weight and Power (SWaP) are not compliant with secondary payload requirements. On the other hand, the recent trends toward LiDAR miniaturization have significantly reduced the SWaP of these systems, making them a more appealing technology than radar for secondary payload applications. Some technological advances are still required, however, before they can be used for long-range detection applications. In the context of passive sensors, optical cameras have already been widely demonstrated for space-based SSA [17–22]. Their major limitation remains their strong dependence on the illumination conditions. For instance, non-visibility conditions occur when objects pass through the Earth shadow region or are located between the observer satellite and the Sun. However, as shown later, this issue is partially reduced since conjuncting objects typically encounter twice per orbit before TCA, thus providing different observation geometries and lighting conditions. An additional interesting option based on optical detection is to exploit the star trackers already onboard satellites to perform the observations during their idle time [17]. This approach has the unique advantage of not requiring a dedicated secondary payload. However, to detect small objects at long distances, these sensors should feature a particularly large optical aperture, larger than that of commonly operated star trackers [22].

3. Database of past conjunctions

The data used in this paper have been collected through the SOCRATES web service [27] offered by the Center for Space Standards & Innovation (CSSI), which every day publishes a list of forecasted conjunctions for the coming week. Besides reporting general information on each event such as the collision probability and the predicted TCA, orbital data are also provided for each object in the form of TLEs, as shown in the example of Fig. 1.

More accurate orbital information on conjunction events could be found in Conjunction Data Messages (CDMs) [28], the standardized text format used worldwide to exchange conjunction notifications. CDMs are regularly issued by the U.S. Space Command (USSPACECOM) to owners/operators of at-risk satellites, who use them to carry out collision avoidance activities. However, there is currently only one large database of publicly available CDMs [29], but it contains partial information that prevents the reconstruction of kinematics before TCA. Conversely, TLEs allow for a straightforward propagation of the orbital states both forwards and backwards in time, but they do not include any uncertainty information. Nevertheless, TLEs error levels have little influence on the results of this paper, as it will be shown in Section 7. A web-scraping algorithm has been used to automatically retrieve data from the website three times per day, that is the rate at which new information is uploaded online, over the period from April 26 to June 7, 2022. Additional data has been collected from past SOCRATES reports dating from January to March 2022.

For a more realistic and meaningful analysis, only high-interest conjunctions meeting specific criteria have been retained, such as a maximum distance at the closest approach of 1 km. To limit propagation error, conjunctions for which the available TLEs were generated more than 2 days before TCA have been discarded. Only events occurring inside Low-Earth Orbit (LEO) have been retained, since it is by far the most congested orbital region and the focus of this paper. Conjunctions between members of the same constellation or in formation flying have also been neglected, as in those cases satellites are more realistically maneuvered frequently to keep safe relative distances. In fact, SOCRATES reports are always more than half occupied by Starlink-Starlink approaches, which however never turn into actual collisions. Finally, to avoid repetitions, only one set of data has been retained per conjunction, since most events appeared several times in subsequent reports following updates on objects' position. The dataset containing the closest information to TCA has been kept for each conjunction. The obtained database includes data on 10,960 unique events, corresponding to 21,920 objects, and is available at Mendeley Data (https://doi.org/10.17632/yfcn6b52yz.1) along with all necessary information for replicating the analyses described in this paper.

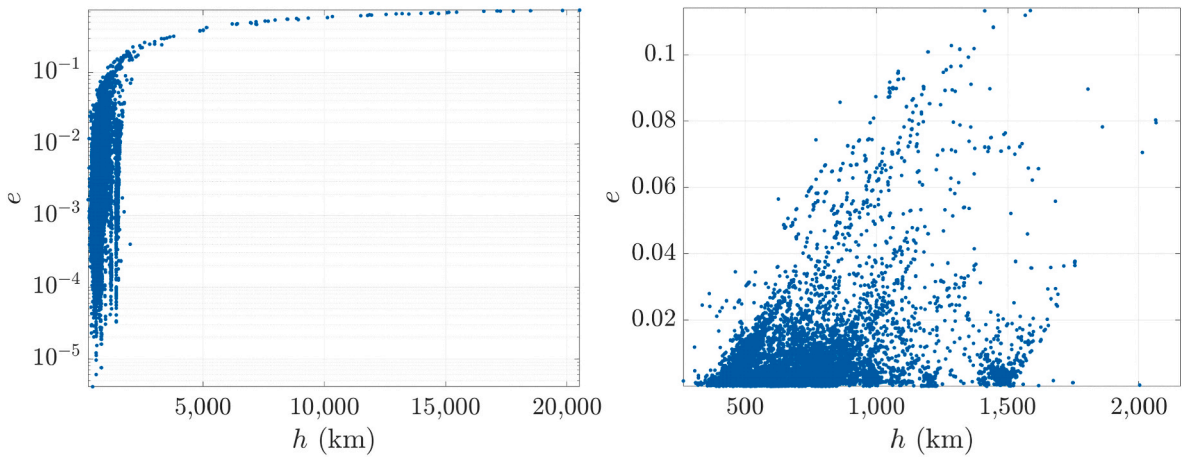

Fig. 2. Mean altitude and eccentricity of the objects. The right plot zooms in on the altitudes below 2000 km.

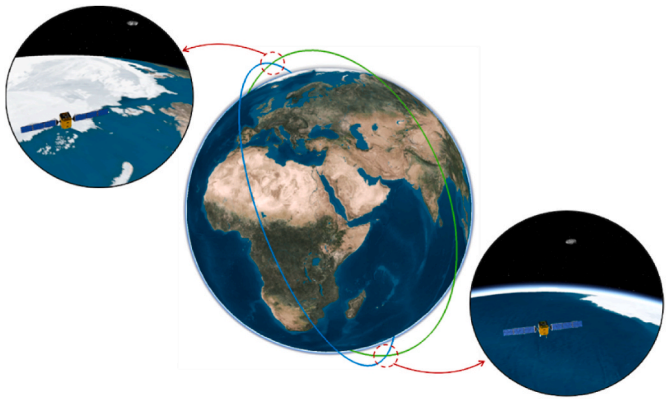

Fig. 3. Typical geometry of conjuncting orbits in LEO.

4. Orbital and kinematics features of conjuncting objects

Fig. 2 shows the distribution of mean altitudes (h) and orbital eccentricities (e) of the objects. h is taken as the difference between the semi-major axis and the equatorial Earth's radius.

As might be expected, most dangerous approaches occur below 1000 km of altitude, where the spatial density is the highest. Conjuncting objects typically have very similar orbital periods, with a difference of less than 1 min in 77% of the cases and less than 2 min in 88% of the cases. In addition, they usually share similar orbital shapes, as 87% of all orbits are nearly-circular ($e < 0.01$) and 96% of the remaining still have moderate eccentricity ($e < 0.1$). Because of these features, conjuncting orbits usually exhibit a similar geometry to that illustrated in Fig. 3, with two points of close orbital proximity on diametrically opposite sides, where the two objects regularly encounter before TCA due to their temporal synchronization. The nearly-periodic nature of this peculiar kinematics is investigated more in detail in Section 4.1.

Although only conjunctions in LEO have been selected, in 0.63% of the cases one of the two objects crosses the LEO region for just a portion of its orbit and has a marked orbital eccentricity. These cases always involve conjuncting objects with quite different orbits and whose motion is significantly out of time phase.

Fig. 4 shows the distribution of relative velocities and impact angles (θ) at TCA. θ is taken as the angle between the projections of the velocity vectors of the two objects on the local horizontal plane of either object, which of the two makes no difference in the analysis. This angle is useful to describe the geometry of a conjunction, which can be categorized as head-on ($135^\circ < \theta < 180^\circ$), cross-track ($45^\circ < \theta < 135^\circ$) or overtaking ($0^\circ < \theta < 45^\circ$).

Since most objects in LEO travel with similar speeds (7–8 km/s), the different values of v_{rel} are mainly due to different conjunction geometries. Fig. 4 shows that most encounters occur with a head-on geometry, i.e., between objects traveling in nearly opposite directions, thus with high relative speeds and kinetic energies.

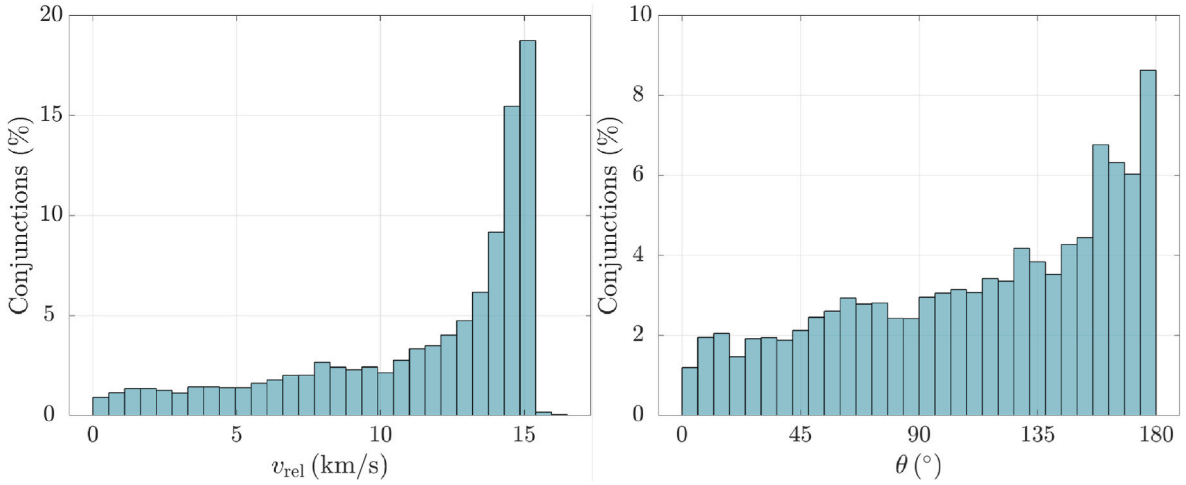

Fig. 4. Relative velocities (*left*) and impact angles (*right*) of conjuncting objects at TCA.

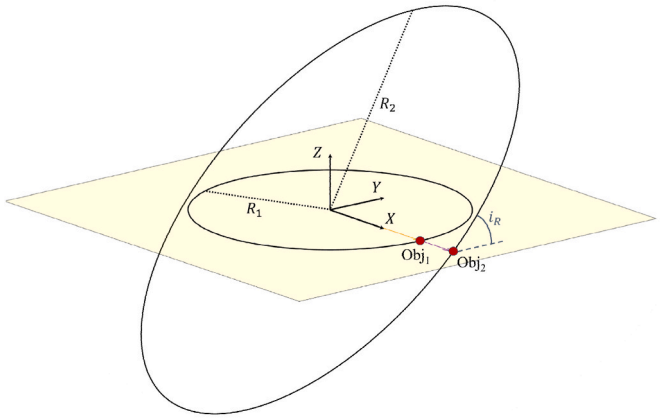

Fig. 5. Position of the two objects at time $t = 0$ relative to the X, Y, Z-reference frame.

4.1. Temporal periodic patterns in the relative motion of conjuncting objects

In this section, a simplified model of the kinematics of conjuncting objects in LEO is used to study the temporal periodic patterns underlying their relative motion. As more than 99% of those objects have moderate eccentricities, the considered model assumes circular Keplerian (i.e., unperturbed) orbits, allowing the problem to be treated analytically while still retaining the necessary accuracy for the analysis.

Consider the motion of two objects in circular orbits of arbitrary radii R_1 and R_2 and whose orbital planes have a relative inclination angle i_R. This latter is defined as the angle between the normal vectors to the orbital planes of the two bodies and can range between 0° and 180° [30]. Referring to Fig. 5, assume a fixed X, Y, Z-coordinate system where the X, Y-axes lie on the first object's orbital plane and the X-axis is aligned with the line of intersection of the two orbital planes. Let $t = 0$ identify the TCA between the objects and assume that both lie on the positive axis X at this time, thus reaching their closest possible distance $(R_2 - R_1)$. Although in reality conjuncting objects do not exactly achieve the minimum possible distance allowed by their orbits, they generally come close to it, especially in particularly high-risk events.

The motion of the two bodies as a function of time can be expressed in the X, Y, Z-reference frame as:

$$\boldsymbol{r}_1(t) = R_1 \begin{bmatrix} \cos(n_1 t) \\ \sin(n_1 t) \\ 0 \end{bmatrix}; \; \boldsymbol{r}_2(t) = R_2 \begin{bmatrix} 1 & 0 & 0 \\ 0 & \cos(i_R) & -\sin(i_R) \\ 0 & \sin(i_R) & \cos(i_R) \end{bmatrix} \begin{bmatrix} \cos(n_2 t) \\ \sin(n_2 t) \\ 0 \end{bmatrix} \tag{1}$$

where n denotes the orbital angular velocity, which is linked to the orbital period T through the relation:

$$n = 2\pi / T \tag{2}$$

As the objects proceed in their orbits, their relative position $\boldsymbol{r}_{\text{rel}}$ is given by:

$$\boldsymbol{r}_{\text{rel}}(t) = \boldsymbol{r}_2(t) - \boldsymbol{r}_1(t) = \begin{bmatrix} R_2 \cos(n_2 t) - R_1 \cos(n_1 t) \\ R_2 \sin(n_2 t) \cos(i_R) - R_1 \sin(n_1 t) \\ R_2 \sin(n_2 t) \sin(i_R) \end{bmatrix} \tag{3}$$

and their separation (or miss-distance) $r_{\text{rel}}(t)$ is simply the norm of $\boldsymbol{r}_{\text{rel}}(t)$. By taking the square of $r_{\text{rel}}(t)$, and after some manipulation, leads to:

$$\begin{aligned} r_{\text{rel}}^2(t) \quad &= R_1^2 + R_2^2 - 2R_1R_2(\cos(n_1 t)\cos(n_2 t) + \cos(i_R)\sin(n_1 t)\sin(n_2 t)) = \\ &= R_1^2 + R_2^2 - 2R_1R_2 \cdot g(t) \end{aligned} \tag{4}$$

It is shown that the function $g(t)$, which groups the time-dependent terms of Eq. (4), can be decomposed into the linear combination of elementary sine and cosine waves with frequencies $n_2 - n_1$ and $n_2 + n_1$, by stating the following problem:

$$g(t) = \sum_{k=1}^{2} \left[a_k \cos\left(\left(n_2 - (-1)^k n_1 \right) t \right) + b_k \sin\left(\left(n_2 - \left(-1^k \right) n_1 \right) t \right) \right] \tag{5}$$

By equating the two expressions of $g(t)$ from Eqs. (4) and (5) and solving for the unknown coefficients a_k, b_k, yields:

$$\begin{cases} a_1 = \dfrac{1 + \cos(i_R)}{2} \\ a_2 = \dfrac{1 - \cos(i_R)}{2} \\ b_1 = b_2 = 0 \end{cases} \tag{6}$$

Hence:

$$g(t) = \frac{1 + \cos(i_R)}{2} \cos\left((n_2 - n_1) t \right) + \frac{1 - \cos(i_R)}{2} \cos\left((n_2 + n_1) t \right) \tag{7}$$

The two frequencies $n_2 - n_1$ and $n_2 + n_1$ can be expressed in terms of the corresponding temporal periods through Eq. (2):

$$\begin{aligned} n_2 - n_1 &= \frac{2\pi}{T_2} - \frac{2\pi}{T_1} = \frac{2\pi}{\dfrac{T_1 T_2}{T_1 - T_2}} = \frac{2\pi}{T_L} \\ n_2 + n_1 &= \frac{2\pi}{T_2} + \frac{2\pi}{T_1} = \frac{2\pi}{\dfrac{T_1 T_2}{T_1 + T_2}} = \frac{2\pi}{T_S} \end{aligned} \tag{8}$$

where the sub-scripts L, S are used to identify the longest and shortest period between the two. Substituting Eqs. (7) and (8) inside Eq. (4) yields:

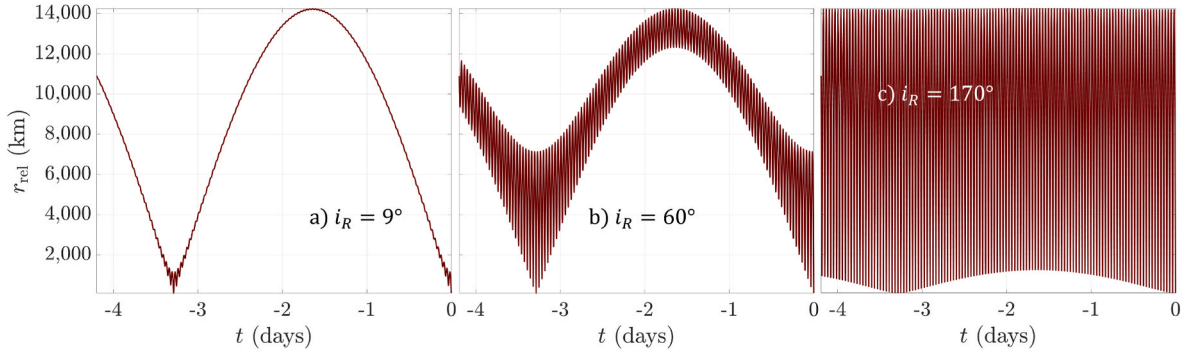

Fig. 6. Miss-distance between two circular Earth orbits with radii $R_1 = r_E + 700$ km and $R_2 = r_E + 800$ km, where r_E is the Earth's radius, considering three values of i_R: a) 9°, b) 60° and c) 170°.

$$r_{rel}^2(t) = R_1^2 + R_2^2 - 2R_1R_2\left[\frac{1+\cos(i_R)}{2}\cos\left(\frac{2\pi}{T_L}t\right) + \frac{1-\cos(i_R)}{2}\cos\left(\frac{2\pi}{T_S}t\right)\right] \quad (9)$$

and so the miss-distance is:

$$r_{rel}(t) = \sqrt{R_1^2 + R_2^2 - 2R_1R_2\left[\frac{1+\cos(i_R)}{2}\cos\left(\frac{2\pi}{T_L}t\right) + \frac{1-\cos(i_R)}{2}\cos\left(\frac{2\pi}{T_S}t\right)\right]} \quad (10)$$

Eq. (9) shows that the evolution of $r_{rel}^2(t)$ is given by the superposition of two sinusoidal functions with different periods (T_L and T_S), whose relative weight depends on i_R. Despite the presence of the square root in Eq. (10), it can be shown that $r_{rel}(t)$ has the same frequency content of $r_{rel}^2(t)$. Indeed, by taking the first derivative of both Eqs. 9 and 10, it can be verified that the functions $r_{rel}^2(t)$ and $r_{rel}(t)$ have the same points of local maxima and local minima, meaning that they feature the same oscillatory pattern.

The superposition of the two sinusoids is evident in the example of Fig. 6, which shows the evolution of r_{rel} prior to TCA ($t < 0$) for two objects orbiting the Earth at 700 km and 800 km of altitudes and considering three different values of i_R. For the considered altitudes, T_L = 3.29 days and T_S = 49.83 min, which reflect the long- and short-period oscillations noticeable in the three graphs.

For i_R close to 0°, i.e., nearly-coplanar orbits with same direction of rotation, $\cos(i_R) \sim 1$ and so the miss-distance is governed by the long periodicity T_L, as in Fig. 6a). This case well reflects, for example, the relative motion between any couple of planets in the Solar System, whose orbits have all the same rotation direction and are close to the ecliptic plane, except for Mercury. In fact, T_L corresponds to the well-known formula of the synodic period, which gives the time required by two planets to return to a same angular position with respect to the Sun. For i_R close to 180°, i.e., nearly-coplanar orbits with opposite direction of rotation, $\cos(i_R) \sim -1$ and the miss-distance is mostly governed by the short periodicity T_S, as shown in Fig. 6c). For each intermediate case, such as that in Fig. 6b), both frequencies are clearly distinguishable in the relative motion.

Regarding conjuncting objects in LEO, i_R can assume all values between 0° and 180°, with a skewed distribution toward $i_R = 180°$. A good approximation of this distribution is given by that of the impact angle θ shown in Fig. 4, given that, for circular orbits, i_R and θ coincide. Therefore, apart from few rare cases where i_R is close to 0°, the contribution of the T_S-periodic sinusoid is always evident the relative motion of conjuncting objects in LEO. In addition, as seen in Section 4, those objects generally feature very similar orbital periods. Considering the limit case $T_1 = T_2$, T_S corresponds to exactly half of the orbital period of the two objects. For these reasons, the relative distance between conjuncting objects typically reach local minima every half-orbit prior to TCA, and more precisely with a periodicity of T_S.

5. Orbit propagation

The trajectory of each couple of conjuncting objects in the database is reconstructed over the 2-days preceding their predicted closest approach. For the orbital propagation, Vallado's Matlab® implementation of the SGP4 propagator [31] is used. SGP4 is an analytical model accounting for the periodic and secular effects caused by atmospheric drag, Earth's oblateness, third body perturbations (Sun and Moon) and gravitational resonance effects. When TLEs are being used, SGP4 is the most faithful propagator as it was specifically designed for use in conjunction with them. Starting from a TLE as input, SGP4 can analytically estimate an object's position $\boldsymbol{r}$ and velocity $\boldsymbol{v}$ at any point in time, without the need for numerical integration.

For each couple of objects, $\boldsymbol{r}$ and $\boldsymbol{v}$ are evaluated at the same time instants, and the relative kinematics is reconstructed in parallel by computing at each point the relative distance r_{rel}, the relative velocity v_{rel} and the angular rate ω. The first two are simply obtained as $\| \boldsymbol{r}_2 - \boldsymbol{r}_1 \|$ and $\| \boldsymbol{v}_2 - \boldsymbol{v}_1 \|$ respectively, where the sub-scripts 1 and 2 denote the two objects. To calculate ω, it is assumed that object 1 (arbitrary choice) is a satellite hosting a tracking sensor whose FoV direction coincides with the surface normal of the satellite's front surface. Identifying with $\hat{s}$ the direction of the sensor axis, ω is calculated at each instant as the time variation of the angle between $\hat{s}$ and the relative position $\boldsymbol{r}_{rel}$. As these two vectors should be aligned as much as possible during an observation window to correctly track the secondary object, ω provides information on how fast a sensor's FoV would need to be rotated in a real scenario. The definition of $\hat{s}$ further assumes that the spacecraft maintains an Earth-pointing attitude orientation, as done by most active satellites in LEO. Whereas, the sensor has been assumed to be mounted on the front surface as this latter is exposed to the highest flux of debris, thus an actual design of the system would most likely lead to mounting the sensor just as described.

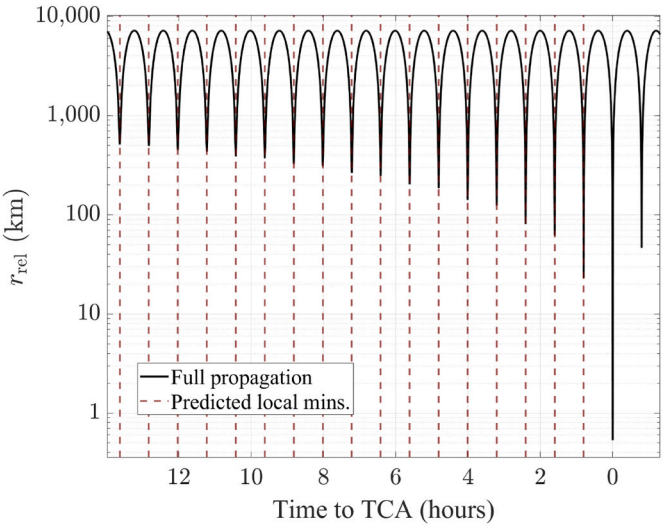

Fig. 7. Fully propagated relative trajectory (*solid line*) vs predicted times of local minima (*dashed lines*).

Given the huge relative velocities of orbital encounters, to correctly evaluate the objects' kinematics a fine propagation time-step (Δt) is required to compute the trajectories. Here, Δt is calculated at each instant so as to always ensure a resolution of 1 km in the computed $r_{rel}(t)$ for each couple of objects. Higher resolutions would make poor sense as TLEs are not generally reliable at a sub-kilometer level [23]. Unfortunately, this leads to evaluate millions of points just for the trajectory of a single object, which translates into a total estimated time of around one month to propagate the entire database. Therefore, a more targeted strategy is used to reduce the computational burden.

As the overall purpose is the characterization of potential observation opportunities, instead of propagating all trajectories over the entire two days preceding TCA, the focus can be placed on the points of local minima of r_{rel}, since there is where the best chances of making observations are. Considering that most orbits have moderate eccentricities and recalling the discussion of Section 4.1, the times of local minima of $r_{rel}(t)$ can be approximately located for each couple of objects as follows:

$$t_{min,j} = \text{TCA} - j \cdot T_S = \text{TCA} - j \cdot \frac{T_1 T_2}{T_1 + T_2} \quad \text{with } j = 1, 2, 3, \ldots \quad (11)$$

where the TCA is known from the database information (see Fig. 1) and the j-loop is stopped when the last computed $t_{min,j}$ is farther than 2 days from TCA. Although Eq. (11) applies primarily to circular orbits, it produces negligible errors when both objects have moderate eccentricities ($e < 0.1$). For example, using Eq. (11) to calculate the local minima for conjunction no. 67 in the database, which involves an object with eccentricity of 0.108, yields a maximum deviation of 2.95 min for one of

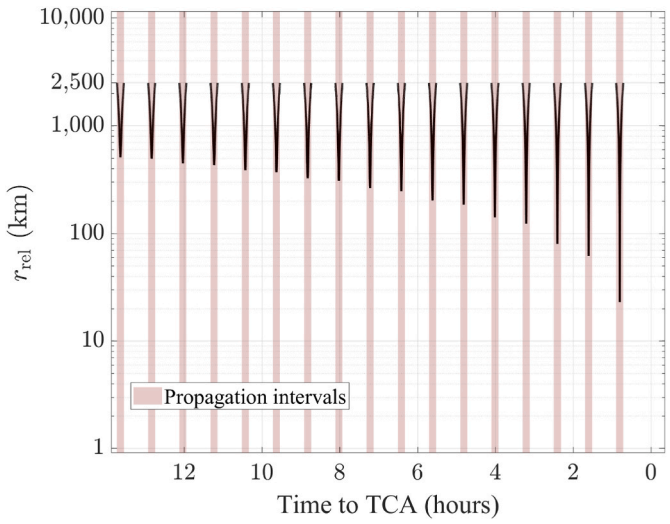

Fig. 8. Propagation intervals.

minima, as in the example of Fig. 8. For each interval, the propagation is stopped at the two points where the miss-distance exceeds 2500 km, a value beyond which it has been assumed that making quality observations becomes difficult for a satellite, especially with a secondary payload. Note from Fig. 8 that the trajectory is not propagated across the global minimum at TCA, because the interest is only on the previous encounters. The above described procedure has been applied for all conjunctions where both objects had a smaller eccentricity than 0.1, for which minimization by Brent's algorithm always succeeded in finding the sought minima. In all other cases (less than 1%), the trajectories have been fully propagated over the two days before TCA.

Fig. 9 shows the evolution of the miss-distance for nine examples of conjunctions from the database.[2] Unlike as seen in the graphs of Fig. 6 obtained with the simplified model, here the local minima do not always decrease monotonically as the TCA approaches. An alternating trend (up and down) between adjacent minima is especially evident in cases a), d), g) and i). It was verified with some simple tests that this effect is due to the non-zero orbital eccentricities of real-world objects, which cause the distance between conjuncting orbits to be slightly different at the two points of proximity where the encounters occur.

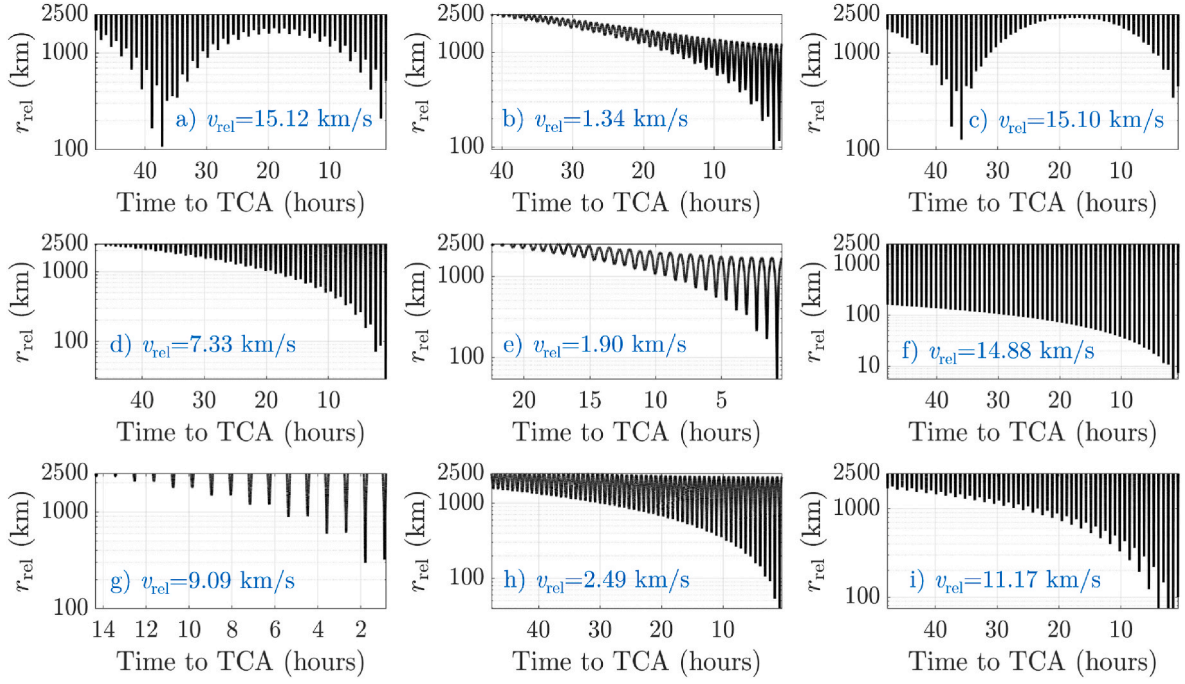

Fig. 9. Miss-distance evolution for a few conjunction events. In blue are reported the relative velocities at TCA. (For interpretation of the references to colour in this figure legend, the reader is referred to the Web version of this article.)

the local minima as compared with the full trajectory solution. Hence, $t_{min,j}$ represent good starting points from which the actual minima are very close. The latter are computed in a second step by locally minimizing r_{rel} on short intervals (±5 min) around each $t_{min,j}$. Here, the minimization is carried out by means of Brent's algorithm for functions of one variable [32], which converges very rapidly to the sought minima. Fig. 7 provides a visual comparison of a point-by-point calculated miss-distance with the location of its local minima obtained using the above procedure.[1] Once the points of true minima are known, the objects' trajectories are only propagated on short intervals around the

Another distinctive feature is shown in cases a) and c), where the two objects experience an additional close approach several hours before the closest one. This occurs when conjuncting objects have a particularly different orbital period, such that the value of T_L (see Eq. (8)) is smaller than the two days time-span considered here, so another close approach is visible in the plots. In fact, orbital periods differ by less than 1 min in all cases of Fig. 9 except for a) and c), where the difference is larger than 4 min, resulting in a T_L of 37.94 h in case a) and 36.43 h in case c). Lastly, it can be noticed that objects with low relative velocities (around 2 km/s) remain in proximity more continuously in the hours before TCA because of their nearly parallel motion in the along-track direction.

[1] The graph has been plotted using conjunction no. 25 from the database, which involves the active Ningxia-1 3 satellite and a piece of debris from the Yuanhai 1–02 satellite.

[2] The graphs correspond in alphabetical order to conjunctions nos. 4014, 40, 37, 153, 91, 3515, 2943, 96, 4007 from the database.

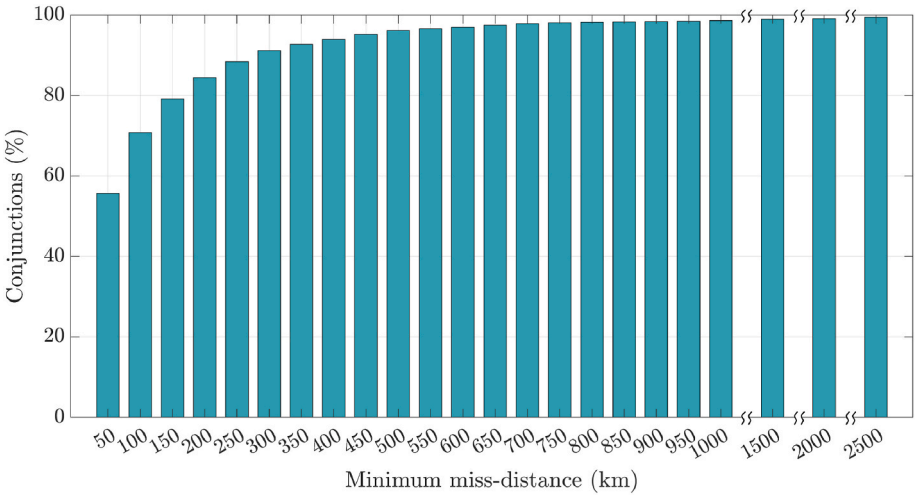

Fig. 10. Minimum miss-distance achieved by conjuncting objects in the two days before TCA (cumulative graph).

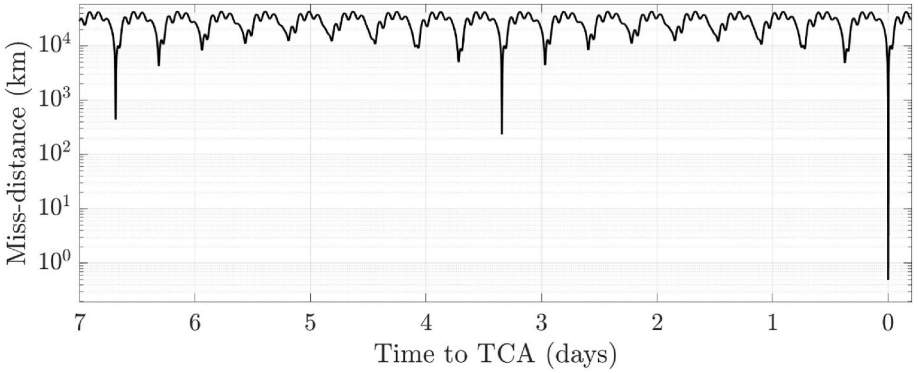

Fig. 11. Relative distance between an object in LEO and one in Molniya orbit.

6. Analysis of observing opportunities

The propagated trajectories are analyzed in terms of relative distances, relative velocities, and other relevant features that contribute to determine whether the repeated encounters between conjuncting objects can actually translate into opportunities for making observations.

6.1. Relative distances

The relative distances are one of the aspects influencing how bright a target object will appear to an observer satellite. Other important factors are the size of the object, its material properties and the Sun phase angle, which is the angle formed between the Sun, the object and the spacecraft. In the case of NEOSSat, objects were regularly detectable from distances spanning 3000 to 4000 km. Nonetheless, the spacecraft was equipped with a 15-cm aperture telescope, whose SWaP is not compliant with the typical requirements of secondary payloads.

An overview of the minimum miss-distances achieved by conjuncting objects in the two days before TCA is shown in Fig. 10. It can be seen that around 70% of the times two objects make a pass at less than 100 km before making the closest approach.

Note that, even if a satellite was able to detect targets at a range of 1000 km, a few secondary objects would still not be visible in the two days before TCA. Closer investigation of these cases revealed that they always involve one object with a marked orbital eccentricity, whose motion is out of phase with respect to that of the other object. An example of such scenario is given in Fig. 11, where one of the objects is a debris from Cosmos 2251 satellite that travels in nearly-circular orbit at

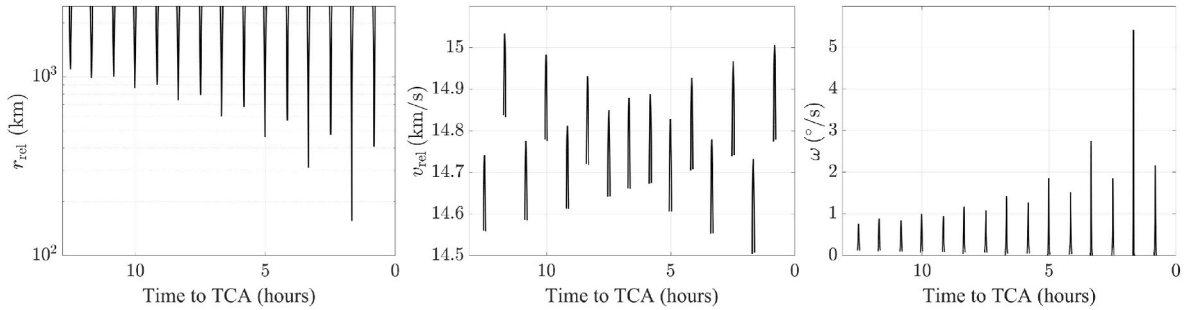

Fig. 12. Evolution of miss-distance (*left*), relative velocity (*center*) and angular rate (*right*) for conjunction no. 6 from the database.

841 km of altitude, while the other is a piece of rocket body in Molniya orbit, with an eccentricity of 0.74 and a semi-major axis of 26,890 km. In this case, the two orbits form a larger synodic period that leads the objects to come close together about once every 3.3 days. A space-based observing strategy here would not bring any particular value over ground-derived data, especially because of the last available observing opportunity being too far away from TCA.

6.2. Relative velocities and angular rates

The example of Fig. 12 shows that the local minima of r_{rel} correspond to local maxima in v_{rel}. Note that, as it is defined, v_{rel} does not coincide with the time derivative of r_{rel}, which would otherwise be zero in correspondence of the local minima of r_{rel}. The pattern of the relative velocity can greatly vary from case to case. A generally valid feature is that during the various encounters before TCA, the velocity reaches peak levels more or less similar to that reached at TCA. In other words, if v_{rel} is 3 km/s at TCA, it is unlikely to reach 15 km/s in the preceding passages. An interesting feature noticeable in Fig. 12 is that the velocity peaks can follow two different trends, one ascending and one descending, looking at the encounters two by two. This can occur when successive passages occur at opposite orbital points. In any case, the design of an onboard sensing system should primarily address relative velocities ranging between 13 and 15 km/s, as most conjunctions occur at those velocities (see Fig. 4) and they pose the biggest technical challenges.

Another key aspect concerns the angular rates experienced during the encounters, which drive important considerations on the pointing performance required to onboard sensing system. The typical pattern of ω is shown on the right of Fig. 12. When two objects are still far apart before a generic encounter, the angular rate is almost null. As they get closer, ω rapidly increases until reaching a sharp peak at the time of minimum distance, after which it decreases again.

The peaks reached by ω during the orbits prior to TCA are typically extremely high. In more than 90% of the conjunctions, ω reaches 100°/s during the encounter occurring one orbit before TCA, if there is one. Encounters with a frontal geometry and involving close relative distances produce the highest values, often reaching over 1000°/s. These angular rates clearly exceed any realistic sensor or attitude pointing control capability. Therefore, the useful time for making observations during an observing window is limited by the maximum angular rate beyond which the observer satellite can no longer track the other object. If an object first becomes visible to the satellite when its angular rate is already too high for tracking, no data can be acquired. In the NEOSSat experiment, the satellite regularly lost track of its conjuncting objects once their relative distance fell below 250 km during the various passes [22].

For the next results, a reasonable threshold limit of 1°/s is assumed beyond which secondary objects are considered not to be visible.

6.3. Time to first opportunity

In order to provide a satellite with sufficient response time to execute a maneuver, observations should not be performed too close to a potential collision. However, the best observing opportunities tend to arise close to TCA, when conjuncting objects typically spend more time in close proximity and their future states can be predicted with greater accuracy. Therefore, the decision on when to execute a maneuver results in a trade-off between the amount of warning time and the probability of a false alert.

Currently, collision avoidance maneuvers are typically performed 0.5–1.5 revolutions before the expected collision by slightly firing in the direction of motion of the spacecraft. Some exceptions exist, but the current general trend is to reduce the time between maneuver execution and potential collision [2]. In order to assess whether close passes before TCA would provide satellites with adequate warning times for maneuvering, an analysis of when secondary objects first become visible before the closest approach has been performed. Encounters where the angular rates were always above a threshold of 1°/s have not been considered as observing opportunities.

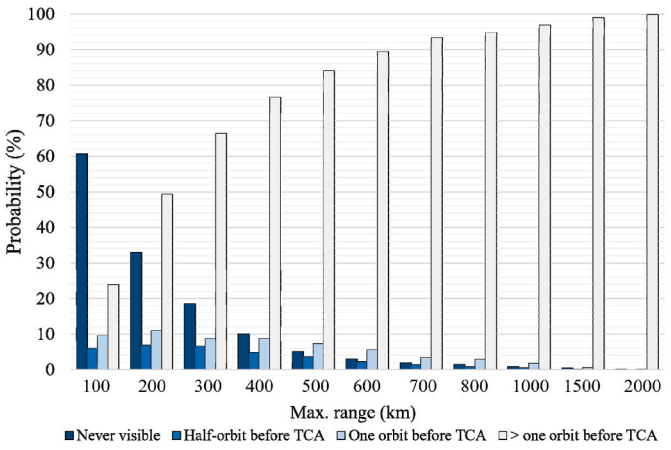

Fig. 13. Probability of when secondary objects first become visible depending on the maximum detection range of the sensor.

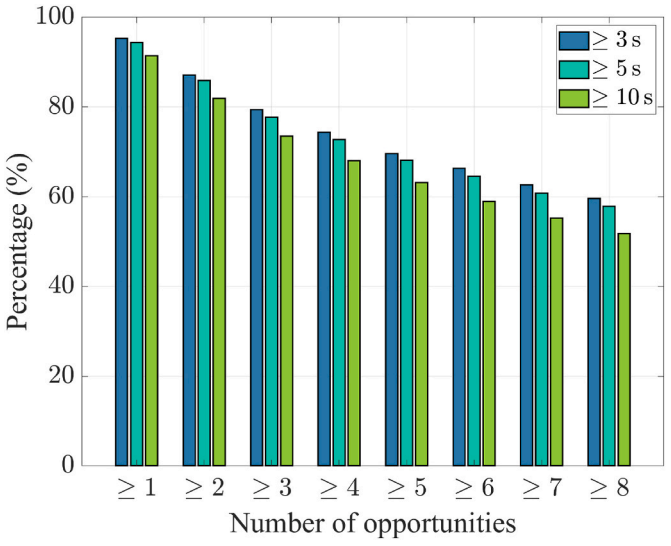

Fig. 14. Number of observing opportunities lasting more than 3 s, 5 s and 10 s during the two days before TCA and considering a maximum detection range of 500 km.

Results shown in Fig. 13 exhibit a strong dependence on the maximum distance at which an observer satellite would be able to distinguish a secondary object. The timings are categorized into four classes to highlight the cases where objects first appear half or one orbit before TCA, i.e., when typically a maneuver decision has already been made. For the lowest values of the detection range considered, most of the objects are never visible and first opportunities tend to cluster towards TCA, making strategies of in-situ observations inefficient. Instead, starting from ranges of 500–600 km, about 90% of secondary objects would be detectable with adequate lead-time.

An interesting aspect can be noticed by comparing Fig. 10 with Fig. 13. Even though 70% of secondary objects pass within a distance of 100 km from their primary before TCA, Fig. 13 by contrast shows that 60% of objects would not be visible with a sensor range of 100 km. This is because most of the encounters below 100 km feature angular rates exceeding 1°/s, and hence do not represent useful opportunities for making observations.

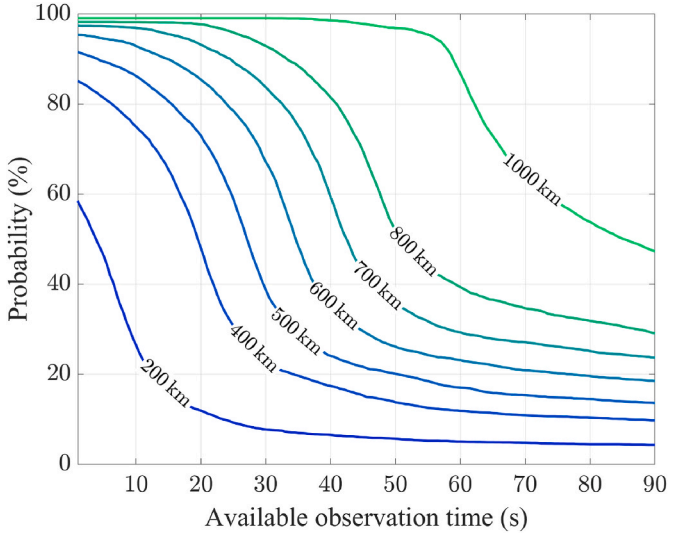

Fig. 15. Duration of the longest observing opportunity depending on the maximum detection range.

6.4. Average number and duration of observing windows

The number and duration of available observing opportunities determine the amount of information that can be collected on a target object. When multiple observation points are available, orbit determination can be performed to a higher confidence level.

Fig. 14 provides a statistic on the number of observation windows arising during the two days before TCA to a satellite that is able to detect targets at 500 km. The graph shows how the number of opportunities varies by selecting different thresholds of the minimum windows duration. The duration has been calculated by considering that each two objects are in visibility from the time their distance falls below 500 km until their angular rate exceeds 1°/s. The FoV of the sensor is assumed to be correctly pointed toward the target at the time the range falls below the selected threshold, since the onboard available orbital data is processed each time to determine the azimuth/elevation sector from where the object is expected to appear. Opportunities occurring half a revolution before TCA have been neglected from the count, assuming that a satellite would have generally already maneuvered by that time. For the considered value of the detection range, at least two opportunities lasting more than 10 s are available in more than 80% of the cases.

Finally, Fig. 15 shows the duration of the longest observing window for each event, considering several detection ranges. Assuming for instance that 10 s is a reasonable enough time for detecting and observing a target object, a range of 600 km guarantees at least one observing opportunity of this kind in about 90% of the cases. By increasing the range to 1000 km, a 1-min opportunity is almost always available.

6.5. Azimuth and elevation angles

Imaging a secondary requires the FoV to be properly aligned with the oncoming object direction. Here, an investigation on the provenance direction of secondary objects during the repeated encounters is done by analyzing their angular position evolution with respect to their primaries. The relative angular position can be expressed in terms of azimuth and elevation angles. The azimuth A ranges from 0° to 360° and is defined within the primary's Local Horizontal Plane (LHP), whose normal vector alignes with the outward radial direction. A is measured clock-wise from the projection of the primary's flight direction onto the LHP to the projection of the relative position vector. The elevation h ranges from −90° to 90° and is defined as the angle between the LHP and the relative position vector. For each couple of objects in the database, the role of secondary one has been assigned randomly.

The $A-h$ evolution can vary significantly depending on the specific trajectories of two objects. A couple of features can be highlighted by examining the values assumed by those angles at different relative distances. Fig. 17 shows the distributions of A and h during the last encounter before TCA and for three different values of r_{rel}. The elevation angle is typically small regardless of the distances, and its distributions are nearly symmetrical around a mean value that changes depending on r_{rel}. h tends to assume values around −10° at distances of 1500 km, but it gradually increases toward 0° as the objects get closer. Analyzing distributions of h at longer distances than 1500 km has shown that the mean value remains close to −10°. Therefore, if a secondary object is visible at distances of >1500 km, it will typically appear from below the LHP of the primary, which should point its FoV at an elevation of about −10°. At a range of 1000 km, the mean elevation is −5°.

The A distributions all cluster towards 0° and 360°, meaning that the encounters prior to TCA are typically characterized by a frontal geometry, similarly to what occurs at TCA. This suggests that a sensor should be oriented in the satellite's direction of motion most of the times.

7. Accuracy of the results

The results of this paper are based on TLE-derived orbits, which have a limited reliability. In general, TLEs accuracy depends on a variety of factors and can greatly change from case to case. Nevertheless, a general rule valid in most cases is that the positional error produced by TLEs for LEO objects can reach 1 km at epoch and grows by 1–3 km per day of propagation, using a SGP4 propagator [24]. On one hand, these error levels are surely not sufficient for estimating the closest distance at TCA, which can reach the meter level. However, during the encounters before TCA, the relative distances are considerably larger and so an error of few kilometers has a much smaller impact.

A simple analysis can be done to assess how the error on object position affects the calculated relative distances, since most of the results in this paper are based on the latter. Denoting with $\boldsymbol{r}_1(t)$ and $\boldsymbol{r}_2(t)$ the nominal positional vectors predicted through TLEs, the true positional vectors can be expressed as:

$$\tilde{\boldsymbol{r}}_1(t) = \boldsymbol{r}_1(t) + \boldsymbol{e}_1(t) \tilde{\boldsymbol{r}}_2(t) = \boldsymbol{r}_2(t) + \boldsymbol{e}_2(t) \tag{12}$$

where $\boldsymbol{e}_1(t)$, $\boldsymbol{e}_2(t)$ are two error vectors, whose magnitude is assumed to be of 1 km at epoch and grows by 3 km per day of propagation. No assumption is made about the orientation of the error vectors, even though it is well known that the error component in the along-track direction is usually significantly greater than that in the other directions. Note that, as all TLEs were generated no more than 2 days away from the TCA, the maximum magnitude that each error vector can reach through propagation is 7 km (1 km + 2 days · 3 km/day). This can only occur for an object whose TLE was generated either exactly at TCA or 2 days before, otherwise the propagation time is always smaller than 2 days. The error between the true relative distance and the predicted one can be computed as:

$$\Delta r_{\mathrm{rel}}(t) = \|\tilde{\boldsymbol{r}}_{\mathrm{rel}}(t)\| - \|\boldsymbol{r}_{\mathrm{rel}}(t)\| = \|\tilde{\boldsymbol{r}}_2(t) - \tilde{\boldsymbol{r}}_1(t)\| - \|\boldsymbol{r}_2(t) - \boldsymbol{r}_1(t)\| \tag{13}$$

By expanding and simplifying Eq. (13) eventually leads to:

$$\Delta r_{\mathrm{rel}}(t) = \sqrt{\|\boldsymbol{r}_{\mathrm{rel}}(t)\|^2 - 2\,\boldsymbol{r}_{\mathrm{rel}}(t)\cdot\boldsymbol{e}_{\mathrm{rel}}(t) + \|\boldsymbol{e}_{\mathrm{rel}}(t)\|^2} - \sqrt{\|\boldsymbol{r}_{\mathrm{rel}}(t)\|^2} \tag{14}$$

where $\boldsymbol{e}_{\mathrm{rel}}(t) = \boldsymbol{e}_2(t) - \boldsymbol{e}_1(t)$. From Eq. (14), it can be verified that the error is maximized when the following two conditions are matched: 1) $\boldsymbol{r}_{\mathrm{rel}}(t)$ is parallel to $\boldsymbol{e}_{\mathrm{rel}}(t)$, and 2) the two error vectors are parallel and opposite. In this case, $\|\boldsymbol{e}_{\mathrm{rel}}(t)\|$ becomes the sum of the magnitudes of the individual error vectors and Eq. (14) reduces to:

$$\Delta r_{\mathrm{rel}}(t) = \sqrt{(\|\boldsymbol{r}_{\mathrm{rel}}(t)\| \pm \|\boldsymbol{e}_{\mathrm{rel}}(t)\|)^2} - \sqrt{\|\boldsymbol{r}_{\mathrm{rel}}(t)\|^2} = \pm\|\boldsymbol{e}_{\mathrm{rel}}(t)\| = \pm(\|\boldsymbol{e}_1(t)\| + \|\boldsymbol{e}_2(t)\|) \tag{15}$$

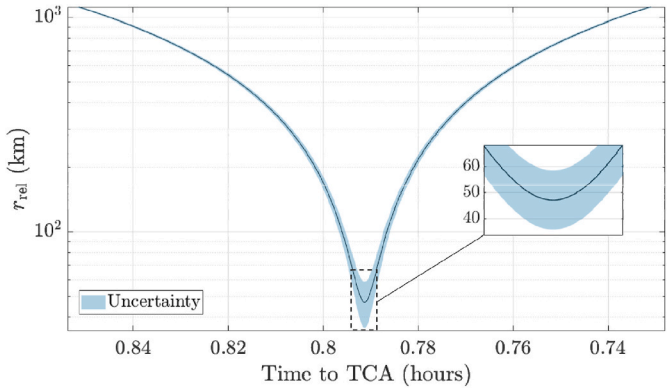

Fig. 16. Uncertainty in the relative distance across a local minimum.

where the $\pm$ accounts for when $\boldsymbol{r}_{\text{rel}}(t)$ is directed in the same or opposite direction to $\boldsymbol{e}_{\text{rel}}(t)$. Eq. (15) has been used to plot the graph in Fig. 16, which shows the relative position uncertainty across a local minimum for a conjunction event from the database. Specifically, the lower and upper limits of the blue region have been computed using Eq. (15) and considering the error growth rule of 3 km/day previously mentioned.

Considering Eq. (15), the maximum theoretical error between the true and the calculated miss-distance is obtained if, in addition to the above two conditions, both objects' TLEs were generated either exactly at TCA or 2 days before. For example, if they were generated 2 days before, the maximum $\Delta r_{\text{rel}}(t)$ possible occurs at TCA and is 14 km (7 km + 7 km). Although several unlikely conditions should align for this case to occur, a distance of 14 km is still small compared to the several hundreds to thousands of kilometers that separate objects during the orbits before TCA. In terms of duration of an observation window, if an encounter occurs with a high relative velocity (12–15 km/s), an error of 14 km on r_{rel} translates into an error of about 1 s on the estimated duration of the window. For lower relative velocities, the error can grow to 4–5 s, but in this case the observing windows tend to last much more, so it would still be negligible.

8. Conclusions

This paper investigated the feasibility of at-risk satellites making autonomous observations of secondary objects during the orbits preceding a probable collision, with the aim of reducing orbital uncertainties and improve risk predictions. Observing opportunities are enabled by the natural motion of conjuncting objects, which typically make several close passes with decreasing relative distances before the closest approach. This peculiar behavior has been studied by reconstructing and analyzing the kinematics of 10,960 past conjunction events, starting from the TLEs of the objects involved.

Since most LEO objects travel in nearly-circular orbits and with similar orbital periods, conjuncting objects tend to meet twice per orbit before the TCA and at opposite nodal intersections, providing valuable observing opportunities with different encounter geometries. A small number (<1%) of conjunctions in LEO involve one object with a marked orbital eccentricity that only passes through this orbital region when close to its perigee. In those cases, observing opportunities are scarce and do not allow for a convenient implementation of the proposed approach. The angular rates achieved by conjuncting objects during the close encounters can easily reach hundreds of degrees per second, making it impossible to continuously maintain a target object within a sensor's FoV. Therefore, an upper limit of 1°/s has been imposed in the calculations to evaluate more realistic trajectory portions for making observations. The results are strongly dependent on the maximum distance at which an onboard sensor is able to distinguish a secondary object. For lower ranges than 300 km, a large amount of conjuncting objects could either not be seen or would first become visible in the very last orbits before TCA, during the moments typically predisposed to maneuver execution. Ranges higher than 500 km are more convenient, since most objects would be visible with sufficient advance to provide an adequate response time to a satellite. One last considered aspect has been the time available for making observations during each close encounter. The study has evidenced that if a payload was able to distinguish any object at a range of 500–600 km, around 90% of the secondaries could be observed for at least 10 s in one of the opportunities available before TCA.

In conclusion, conjuncting objects in LEO consistently perform several close passes before a potential collision. The exploitability of these encounters for making in-situ observations depends on various factors, among which stands out the capability of the onboard sensor to distinguish objects at a long range. As the relative distances are in the hundreds/thousands of kilometers range, the most viable option at the current state of technology is represented by optical-based sensor systems, which have already been tested in-orbit for SSA purpose. Starting from this initial study, other technical challenges should be addressed in order to determine the optimal technological requirements for the system. For instance, a major problem for optical payloads concerns the illumination conditions of the sensed objects. However, this issue is partially reduced by the fact that there are typically two orbital points where a secondary object can be observed, which are unlikely to be both in an Earth shadow zone.

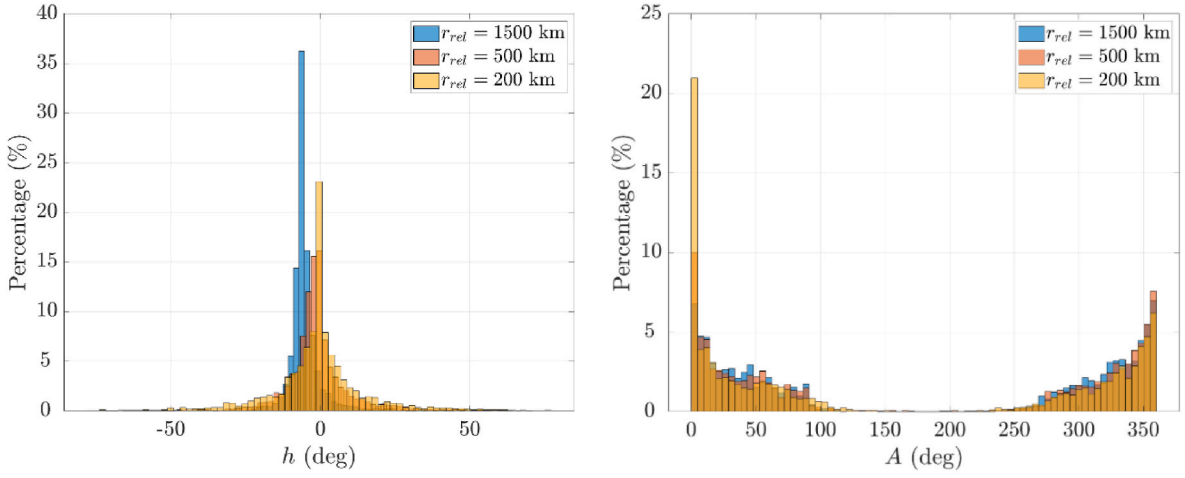

Fig. 17. Distribution of h (*left*) and A (*right*) at the last encounter prior to TCA.

Declaration of competing interest

The authors declare that they have no known competing financial interests or personal relationships that could have appeared to influence the work reported in this paper.

Acknowledgements

We thank Dr. T. S. Kelso, the webmaster of SOCRATES service, for providing access to archived documentation on historical conjunctions not directly available from the website. We also thank M. Tagliente for providing useful suggestions throughout the research. This research did not receive any specific grant from funding agencies in the public, commercial, or not-for-profit sectors.

References

[1] S. Lemmens, F. Letizia, ESA's Annual Space Environment Report, Tech. Rep. GEN-DB-LOG-00288-OPS-SD, ESA Space Debris Office, Darmstadt, Germany, 2022.
[2] T. Flohrer, H. Krag, K. Merz, S. Lemmens, Cream - ESA's proposal for collision risk estimation and automated mitigation, in: Proceedings of the Advanced Maui Optical and Space Surveillance Technologies Conference, AMOS), 2019.
[3] European Space Agency, "ESA & UNOOSA Space Debris Infographics and Podcast", Accessed 18 Jan 2023, https://www.esa.int/Space_Safety/Space_Debris/ESA_UNOOSA_space_debris_infographics_and_podcast>.
[4] European Space Agency, *"Sentinel Online – News"*, Accessed 18 Jan 2023, <https://sentinels.copernicus.eu/web/sentinel/-/copernicus-sentinel-1a-collision-avoidance-manoeuvres-on-16-may-2022/1.1≥.
[5] Edouard Mathieu and Max Roser, *"Space Exploration Satellites"*, Our World in Data, Accessed 18 Jan 2023, <https://ourworldindata.org/space-exploration-satellites≥.
[6] S. Hilton, F. Cairola, A. Gardi, R. Sabatini, N. Pongsakornsathien, N. Ezer, Uncertainty quantification for space situational awareness and traffic management, Sensors 19 (20) (2019) 4361–4384.
[7] V. Braun, A. Horstmann, S. Lemmens, C. Wiedemann, L. Böttcher, Recent developments in space debris environment modelling, verification and validation with MASTER, 8(1), in: T. Flohrer, S. Lemmens, F. Schmitz (Eds.), Proceedings of the 8th European Conference on Space Debris, ESA Space Debris Office, Darmstadt, Germany, 2021.
[8] European Space Agency, Online Space Debris Training Course 2022, Lecture one: Introduction, 2022.
[9] S.J. Setty, T. Flohrer, H. Krag, SLR for space debris monitoring: an analysis on requirements and achievable orbit improvement, in: T. Flohrer, R. Jehn, F. Schmitz (Eds.), Proceedings of the 1st NEO and Debris Detection Conference, ESA Space Safety Programme Office, Darmstadt, Germany, 2019.
[10] L. Mariani, G. Zarcone, F. Santoni, G. Bianchi, M. Acernese, M.F. Montaruli, P. Di Lizia, F. Piergentili, F. Curianò, S.H. Hossein, Enhancing the knowledge on space debris attitude and position combining radar and optical observations, in: S. Lemmens, F. Schmitz (Eds.), *8th European Conference On Space Debris*, Flohrer T., ESA Space Debris Office, Darmstadt, Germany, 2021.
[11] D.L. Oltrogge, P. Wauthier, D.A. Vallado, S. Alfano, T.S. Kelso, Results of comprehensive STCM data fusion experiment, in: S. Lemmens, F. Schmitz (Eds.), *8th European Conference On Space Debris*, Flohrer T., ESA Space Debris Office, Darmstadt, Germany, 2021.
[12] K.M. Keller, D. Yeung, D. Baiocchi, W. Welser IV, Tech. Rep, in: Facilitating Information Sharing across the International Space Community: Lessons from Behavioral Science, RAND Corporation, Santa Monica, California, USA, 2013.
[13] D. Vallado, J. Woodburn, F. Deleflie, Sequential orbit determination using satellite laser ranging, Adv. Astronaut. Sci. Series 152 (2014) 1273–1290.
[14] N. Bartels, P. Allenspacher, D. Hampf, B. Heidenreich, D. Keil, E. Schafer, W. Riede, Space object identification via polarimetric satellite laser ranging, Commun. Eng. 1 (5) (2022).
[15] C. Bamann, U. Hugentobler, Accurate orbit determination of space debris with laser tracking, 7(1), in: T. Flohrer, F. Schmitz (Eds.), Proceedings of the 7th European Conference on Space Debris, ESA Space Debris Office, Darmstadt, Germany, 2017.
[16] E. Cordelli, A. Vananti, T. Schildknecht, Analysis of laser ranges and angular measurements data fusion for space debris orbit determination, Adv. Space Res. 65 (1) (2020) 419–434.
[17] D. Spiller, E. Magionami, V. Schiattarella, F. Curti, C. Facchinetti, L. Ansalone, A. Tuozzi, On-orbit recognition of resident space objects by using star trackers, Acta Astronaut. 177 (2020) 478–496.
[18] R. Ahmed, N. Majurec, J.W. De Bleser, A Cubesat-based radar for characterization of millimetric orbital debris, LPI Contrib. 2109 (1) (2019) 6079.
[19] D. Cerutti-Maori, J. Rosebrock, L. Leushacke, H. Krag, Preliminary concept of a space-based radar for detecting mm-size space debris, 7(1), in: T. Flohrer, F. Schmitz (Eds.), Proceedings of the 7th European Conference on Space Debris, ESA Space Debris Office, Darmstadt, Germany, 2017.
[20] C.R. Englert, J. Timothy Bays, K.D. Marr, C.M. Brown, A.C. Nicholas, T.T. Finne, Optical orbital debris spotter, Acta Astronaut. 104 (1) (2014) 99–105.
[21] ESA/ESOC Space Debris Office, Debris Risk Assessment and Mitigation Analysis (DRAMA) Software User Manual, Tech. Rep. MIT-COL-MAN-00279-OPS-SD, ESA/ESOC Space Debris Office, Darmstadt, Germany, 2020.
[22] R.L. Scott, S. Thorsteinson, V. Abbasi, On-orbit observations of conjuncting space objects prior to the time of closest approach, J. Astronaut. Sci. 67 (4) (2020) 1735–1754.
[23] D. Vallado, P. Cefola, Two-line element sets — practice and use, in: Proceedings of the 63rd International Astronautical Congress, Naples, Italy, 7, 2012, pp. 5812–5825, 1.
[24] D. Vallado, P. Crawford, R. Hujsak, T.S. Kelso, Revisiting spacetrack report #3, in: Proceedings of the AIAA/AAS Astrodynamics Specialist Conference and Exhibit, Keystone, Colorado, USA, 2006.
[25] U.S. Space, Force's 18th Space Control Squadron, Spaceflight safety handbook for satellite operators, Tech. Report, 2020 version 1.5.
[26] S. Alfano, D. Oltrogge, L. Arona, Operators' requirements for SSA services, J. Astronaut. Sci. 69 (5) (2022) 1441–1476.
[27] Kelso, T. S. SOCRATES, Celestrak, Accessed 18 Jan 2023, <https://celestrak.com/SOCRATES/≥.
[28] Consultative committee for space data systems (CCSDS), conjunction data message (blue book), Recommended Standard CCSDS 508.0-B-1, Washington D.C., USA, 2013.
[29] ESA Advanced Concepts Team, "*Collision Avoidance Challenge*", Kelvins - ESA's Advanced Concepts Competition Website, Accessed 18 Jan 2023, <https://kelvins.esa.int/collision-avoidance-challenge/data≥.
[30] L. Chen, X.-Z. Bai, Y.-G. Liang, K.-B. Li, Chapter 4 - close approach analysis between space object, in: Orbital Data Applications for Space Objects, Springer, Singapore, 2017, 978-981-10-2962-2.
[31] D.A. Vallado, P. Crawford, SGP4 orbit determination, in: Proceedings of the AIAA/AAS Astrodynamics Specialist Conference and Exhibit, Reston, Virginia, USA, 2008.
[32] R.P. Brent, Algorithms for Minimization without Derivatives, Prentice-Hall, Englewood Cliffs, New Jersey, USA, 1973, 0-13-022335-2.